Directly imprinted periodic corrugation on ultrathin metallic electrode for enhanced light extraction in organic light-emitting devices

Chi Ma, Xiu-Min Gao, Yan-Gang Bi, Fang-Shun Yi , Xu-Lin Zhang, Da Yin, Yue-Feng Liu, Jing Feng, and Hong-Bo Sun, *Fellow, IEEE*

Abstract—A micro/nano structure on the metallic electrode is necessary to outcouple power lost to surface-plasmon polaritons (SPPs) in organic light-emitting devices (OLEDs). However, a simple and efficient method to integrate the micro/nano pattern onto the surface of the metallic film is still a challenge. In this work, thermal nanoimprint lithography has been employed to directly imprint periodic corrugation onto an ultrathin metallic film. Both surface morphology and conductivity of corrugated metallic film have been improved by the imprinting process, which is important for its use as electrode in optoelectronic devices. The photons that trapped in SPP modes associated at the organic-cathode interface in the OLEDs have been efficiently extracted by using the periodically corrugated ultrathin metallic film as anode of the OLEDs. A 56% enhancement of current efficiency was achieved compared with the planar device. The corrugated ultrathin anode is further applied to flexible OLEDs, and improved light extraction efficiency has been obtained.

Index Terms—ultrathin metallic electrode, periodic corrugation, organic light-emitting devices, light extraction

I. INTRODUCTION

Organic light emitting devices (OLEDs), with advantages of low power consumption, wide view angle and broad color gamut, have been broadly investigated for the next-generation full-color information display and large-area lighting applications[1-5]. However, the light extraction is generally lower than 20 %, which has been the main bottlenecks to achieve excellent performance OLEDs. The indium-tin-oxide (ITO) [6-9] is the most commonly used transparent conductive electrode (TCE) in OLEDs, but its high refractive index will results in power lost to waveguide mode. Moreover, it is suffering disadvantages of high cost and frangibility. Therefore, numerous alternative materials have been developed as substitutions for the ITO electrode, such as conducting polymers[10-13], graphene[14-16], carbon nanotubes[17, 18],

metal nanowires[5, 19, 20] and ultrathin metallic films[1, 21, 22]. Among them, the ultrathin metallic film with excellent mechanical robustness, high transmittance and conductivity has been considered as one of the candidate electrodes for the OLEDs. However, the surface plasmon-polariton (SPP) modes generated between the metallic cathode and organic layer still caused great power loss and significantly limit OLEDs efficiency. On the other hand, the Volmer-Weber [23] growth mode of the evaporated ultrathin metallic film results in its rough morphology and poor electrical conductivity.

Fabricating the wavelength-scale periodic corrugation onto the metallic film is necessary to excite and out-couple the SPP modes, which is caused by giving an additional momentum to out-couple the SPP modes into light. However, the corrugations are usually introduced onto the substrate by using the conventional microstructure fabrication methods in OLEDs, such as laser ablation [24], reactive ion beam etching [25] and two-beam interference lithography [26] et al. For example, Li et al. [27] have successfully fabricated the micro-nano patterns on a surface to realize the flexible adjustment of surface properties. The surface roughness of the deposited metallic electrode on the substrate would be increased by using this strategy and results in declined carrier injecting efficiency and reduced stability of the OLEDs. Introducing the periodic corrugation directly onto the metallic electrode with continuity and smooth morphology is an ideal strategy to out-couple the SPP loss [28, 29] and maintain the efficient carrier injection. However, a simple method to realize the periodically corrugated metallic film is still a challenge.

In this work, the grating configuration with suitable period has been directly imprinted on the surface of the ultrathin metallic film by a simple thermal nanoimprint lithography process. Both surface morphology and conductivity of the corrugated metallic film are improved by the imprinting process. The sheet resistance was decreases from 60 Ω sq^{-1} for the planar film to 28 Ω sq^{-1} for the imprinted film. Using the periodically corrugated ultrathin metallic film as anode of the OLEDs, the corrugated profile was formed throughout each layer of the devices. Through fabricating the nano-scale grating configuration in the device, the trapped photons associated with the SPP modes between the metallic cathode and organic layer in OLEDs have been efficiently extracted and 56% enhanced current efficiency was achieved compared with the planar device. The imprinted metallic anode is applicable to flexible

Chi Ma, Xiu-Min Gao, Yan-Gang Bi , Fang-Shun Yi , Xu-Lin Zhang, Da Yin, Yue-Feng Liu, Jing Feng, and Hong-Bo Sun are with State Key Lab of Integrated Optoelectronics, College of Electronic Science and Engineering, Jilin University, 2699 Qianjin Street, Changchun 130012, China. E-mail: jingfeng@jlu.edu.cn (Correspondence to Prof. J. Feng)

Hong-Bo Sun is also with State Key Lab of Precision Measurement Technology and Instruments, Department of Precision Instrument, Tsinghua University, Haidian, Beijing 100084, China.

This paper has supplementary downloadable material available at http://ieeexplore.ieee.org, provided by the authors.

OLEDs to improve the light extraction.

II. Experiment

A. Fabrication of ultrathin Au-Ag composite film

The glass substrates were pre-cleaned by ultrasonic in acetone, alcohol and de-ionized water, respectively, each step of the cleaning was maintained for twenty minutes. The SU-8 2025 photoresist (MicroChem Corp.) was diluted using the cyclopentanone to relative low concentration of 100 mg/mL^{-1}. Then directly spin-coating to the pre-cleaned glass substrate with 2000 rpm for 30 s, which will lead the final film thickness to around 200 nm. Before the deposition of metallic film, the SU-8 modified glass substrates were transferred into oven to be prebaked at 95°C for 20 min. The 1 nm Ag and 7 nm Au films were deposited in the thermal evaporation chamber, during the deposition process the chamber pressure was maintained below 5×10^{-4} Pa, the deposition rates were set as 1 Å s^{-1} and 0.5 Å s^{-1}. The deposition rate and film thickness were monitored by quartz crystal oscillator. The surface morphologies were detected by atomic force microscope (Dimension Icon, Bruker) and scanning electron microscope (JSM-7500F, JEOL). The sheet resistance was measured by the Four-point probe system. The UV-Vis spectrophotometer (UV-2550, SHIMADZU) was used to detect the transmittance (400 nm-800 nm) of ultrathin metallic film.

B. Fabrication of single-periodic grating configuration

The Si template with serious of fixed periodic gratings was applied as the original template. The prepared polydimethylsiloxane (PDMS) DC184 (Dow Corning Inc) was placed on the Si template. Then, the template was transferred into the vacuum chamber and kept the air pressure below 5×10^{-4} Pa for 30 min to remove the bubbles. After that, the template was moved into the oven for solidification, which was set as 95°C for 3 hours. The cured PDMS template was peeled off from the silicon wafer, covering onto the SU-8 modified glass substrate. The PDMS/SU-8/glass was moved into the Nano-imprinting Machine (CNI1-5vac), which was purchased from NIL Technology Company, setting the temperature, pressure and time as 100°C, 5 bar and 30 min, respectively. Finally, removing PDMS template and exposing under the ultraviolet light source for 30 s with the power of 125 W to solidify the SU-8 photoresist. In the modified method, the thermal nanoimprint process was directly applied on the metallic film/SU-8/glass substrate, and the other parameters remain unchanged.

C. Fabrication and characterization of OLEDs.

The planar and periodic OLEDs were fabricated by physical vapor deposition method. The 1 nm Ag was precoated on SU-8 film act as a seed layer before the deposition of 7 nm Au. A 3 nm MoO$_3$ film was chosen to act as an anodic buffer layer. Then, the 40 nm N,N′-Diphenyl-N,N′-bis(1,1′-biphenyl)-4,4′-diamine (NPB) was chosen as the hole transport layer. The orange phosphorescent emitter Bis(2-phenylbenzothiazolato)(acetylacetonate)iridium(III) (Ir(BT)$_2$(acac)) with a ratio of 5 wt% was co-deposited into the host material 4,4′-Bis(N-carbazolyl)-1,1′-biphenyl (CBP) to act as emitting layer. The hole-blocking layer was 30 nm 2,2′,2″ (1,3,5-benzenetriyl)tris-[1-phenyl-1Hbenzimidazole] (TPBi). Finally, 1 nm LiF combined with 80 nm Al were served as the cathode. The shadow mask was applied to control the pattern of each layer in the chamber. During the whole evaporation process, the pressure in the chamber was maintained below 5×10^{-4} Pa. Therefore, the basic structure of OLED is glass substrate/SU-8/Ag (1 nm)/Au (7 nm) (planar or corrugated)/MoO$_3$ (3 nm)/NPB (40 nm)/Ir(BT)$_2$(acac):CBP (5 wt%, 30 nm)/TPBi (30 nm)/LiF (1 nm)/Al (80 nm). The effective light-emitting area of the device is 4 mm^2, which is controlled by the cross-section of the anode and cathode. The angular dependent EL spectra were measured by Photo Research PR-655 spectrophotometer, and the OLEDs were placed on a rotation stage with grooves parallel to the rotation axis. The polarized TM and TE EL spectra were measured by employing a polarizer between the OLEDs and the spectrophotometer. The current density-luminance characteristics of the devices were measured by Keithley 2400 programmable voltage-current source and Photo Research PR-655 spectrophotometer. All the data were measured in air and room temperature with standard atmospheric pressure.

D. Fabrication of flexible OLEDs.

The glass substrate was pre-cleaned as mentioned above, and then the hydrophobic surface was obtained through vapor depositing Octadecyltrichlorosilane (OTS). The whole deposition process was kept 4 h at 60 °C in the vacuum drying chamber. After that, the glass substrate was scrubbed with acetone, ethanol and flushed with deionized water. Then spin-coating the NOA-63 photoresist to the OTS-modified glass with 2000rpm for 45s. The solidification was carried out by UV light source (125W, 1min). The thickness of solidified NOA-63 flexible substrate is about 30 μm. Then the planar and corrugated OLEDs were fabricated on the NOA-63 substrate as previously stated. When the whole device fabrication is complete, the OLED with flexible substrate can be easily peeled off from the OTS-modified glass.

III. Results and discussions

The thermal nanoimprint lithography, as an effective method to fabricate microstructures, have been deeply investigated and widely used. Usually, the thermal nanoimprint is employed to fabricate the corrugated metallic film by directly imprinting the uncured polymer film (SU-8) and the depositing metallic film would duplicate the corrugation by thermal evaporation, which is marked as imprinted SU-8 in Fig. 1. Different from this conventional process, the fabrication of the corrugated metallic film by the thermal nanoimprint process is modified by depositing an ultrathin metallic film on the planar polymer film of SU-8 before the imprinting, and then the metallic film on the SU-8 are imprinted together, which is marked as imprinted Au in Fig. 1. The Si template with fixed grating periods has been used as the basic template. And the silicon polymer, polydimethylsiloxane (PDMS), was applied to transfer the

grating configuration. The surface morphologies of Si and PDMS template were measured by AFM (Fig. S1), and both have a regular grating structure and the depths are 78 nm (Si) and 63 nm (PDMS), respectively, indicating that the PDMS replicates the microstructure on the silicon template well. The ultrathin metallic film was firstly optimized to obtain high conductivity and transparency (Fig. S2 and S3). Before the deposition of 7 nm Au, the 1 nm Ag was precoated on the SU-8 film act as a seed layer to realize a continuous and highly conductive Au film. The transmittance of the Au/Ag composite film at 550 nm is 78.2% and the sheet resistance is 60 Ω sq^{-1}.
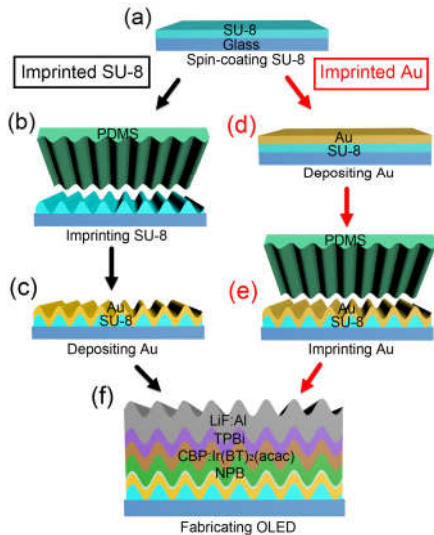

Fig. 1. Schematic of the fabrication process. (a) Spin-coating SU-8 on the glass substrate, (b) imprinting grating configuration onto the uncured SU-8 film, (c) depositing Au film on the grating SU-8 substrate, (d) depositing Au film on the planar SU-8 substrate, (e) imprinting grating configuration onto Au film, (f) fabricating the OLED.

The surface morphologies of the ultrathin composite metallic films with the imprinted gratings are characterized by the AFM and SEM and shown in Fig. 2. The grating configurations fabricated by the two different processes both show good regularity with the grating depth of around 60 nm. However, different surface morphologies of the corrugations can be observed. The duty ratio (the ratio of convex portion of the grating to the grating period) is decreased from 0.58 for imprinted SU-8 to 0.42 for imprinted Au, which has no obvious effect on the device performance. The smoothness of the metallic film on the top of the grating lines is obviously improved for the imprinted Au (insets in Fig. 2a and b). The metallic film is deposited on the corrugated SU-8 for the imprinted SU8 process, and the wavelength-scale terrain difference, such as facet, edge and corner of the gratings, means inhomogeneous surface energy landscape, and eventually lead to the uneven deposition of the metallic film. While in case of imprinted Au, the metallic film is directly deposited onto the planar SU-8, avoiding the adverse effect of the microstructured substrate on the growth of the metallic film. On the other hand, during the nanoimprint process, the high temperature (100℃) and pressure (5 bar) make the fine cracks aggregate into bigger ones, which further optimize the surface morphology of the corrugated metallic film. Moreover, the conductivity of the corrugated metallic films with various Au thickness fabricated

by imprinted Au are much improved compared to that by imprinted SU-8 as can be seen from Fig. 3 (a). Taking 7 nm Au film as an example, the sheet resistance of planar film is 60 Ω sq^{-1}. The sheet resistance is increased to 104 Ω sq^{-1} for the corrugated film fabricated through imprinted SU-8. While it is decreased to 28 Ω sq^{-1} for the directly imprinted Au film, which is even lower than that of the planar film. The much improved conductivity can be attributed to the improved surface morphology.
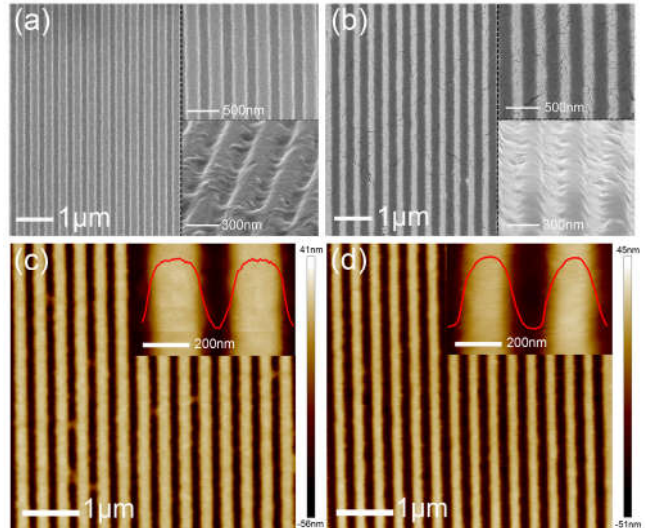

Fig. 2. The SEM (a) and AFM (c) images of Au (7 nm)/ Ag (1 nm) composite grating film fabricated through imprinting SU-8; The SEM (b) and AFM (d) images of Au (7 nm)/ Ag (1 nm) composite grating film fabricated through imprinting Au. The insets in (c) and (d) show the enlarged area of the corrugated metallic films.

The directly imprinted ultrathin metallic film with 7 nm Au on the 1 nm Ag seed layer has been employed in OLED as the bottom anode. The corrugated profile on the anode can be duplicated to the following deposited organic functional and metallic cathode layers by the vapor evaporation. The SPP resonance at interface of organic layer and cathode is tunable by adjusting the grating period. The absorption spectra with grating period changes from 310 nm to 350 nm have been measured and shown in Fig. 3 (b). The planar OLED with the same device structure is set as standard sample to eliminate the influence of metallic and organic layers on the absorption measurement.
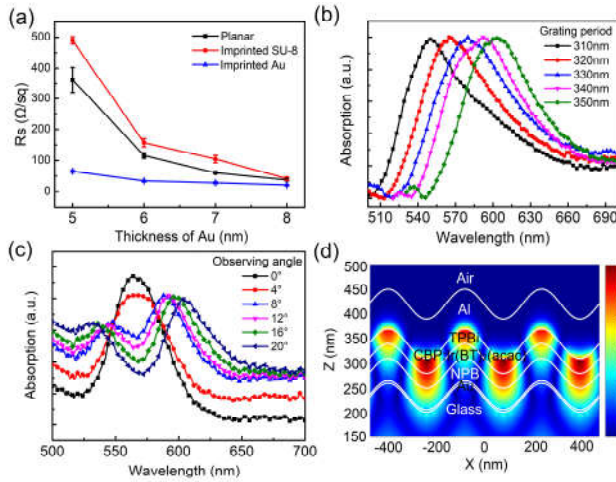
Fig. 3. (a)The sheet resistance with various Au thickness. (b) The absorption spectra of the corrugated OLED structures with grating periods from 310 nm to 350 nm. (c) The angular dependent absorption spectra of the corrugated OLED structures with grating period of 320 nm. (d) The distribution of the magnetic field intensity across the corrugated OLEDs with the normal incident light at 565 nm with TM polarization.

Therefore, it can be confirmed that the absorption peaks is generated form the SPP resonance between the metallic cathode and organic layers. In the absorption measurement, the thickness of Al cathode was decreased to 30 nm. The emission peak of orange phosphorescent emitter $Ir(BT)_2(acac)$ employed in the OLEDs is located at 564 nm (Fig. S5). In order to effectively outcoupling the SPP modes, it is crucial to make sure the SPP resonance to be consist with the emission peak of the OLEDs. The peak wavelength of the absorption is increasing with the increased grating period. It is tuned to close to the emission peak of the OLEDs (565 nm) for grating period of 320 nm. With the increasing of the observing angles, the peak of absorption spectrum splits into two peaks, which is the characterization of the SPP mode. The in-house generated finite difference time domain (FDTD) codes are employed to establish the SPP modes supported by the corrugated structures. The peak wavelengths of the simulated p-polarized absorption spectra are in good accordance with the experimental values (Fig. S6). The TM polarized field intensity distribution at the wavelength of 565 nm for the periodic corrugated OLED is simulated and shown in Fig. 3 (d). The maximum field intensity is located between the Al cathode and organic layer, and gradually decays along the direction perpendicular to the interface. Indicating the absorption peak (565 nm) is generated from SPP modes located at the cathode/organic interface. Based on above results, the corrugation period of 320 nm is appropriate to effectively excite and out-couple the SPP modes in the OLEDs.
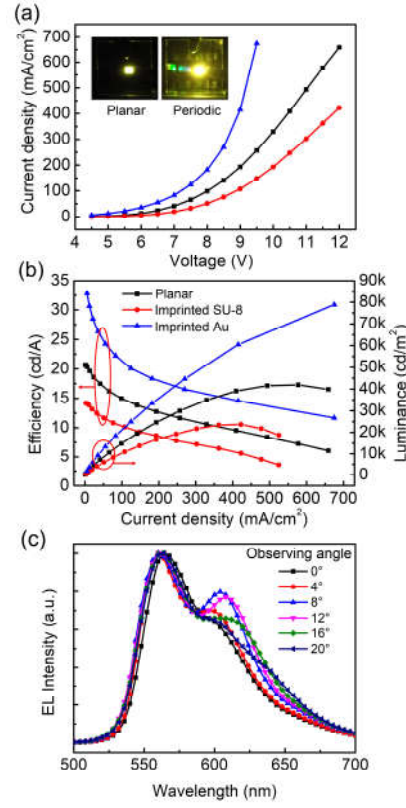

Fig. 4. Electro-luminance performance of the OLEDs with the planar and corrugated Au anode. (a) Current density-driving voltage characteristics. The inset shows the photographs of OLEDs with planar and directly imprinted Au anode at same operating of 5V. (b) Luminance-efficiency-driving current density characteristics. (c) The TM polarized electroluminescent (EL) spectrum of mono-periodic-corrugated OLED with different observing angles.

The EL performance of the grating OLEDs with the period of 320 nm and the planar OLEDs are summarized and shown in Fig. 4. For the planar device, the maximum luminance is 41940 cd m^{-2} and the current efficiency is 20.69 cd A^{-1} (Fig. 4 (b)). The corrugated OLED based on the imprinted SU-8 exhibits the deteriorated performance compared to the planar devices. The maximum luminance and current efficiency are dropped to 23690 cd m^{-2} and 14.16 cd A^{-1}, respectively. This decrease in device performance may be caused by deterioration of the anode surface topography. The corrugated OLEDs with the directly imprinted Au anode exhibit the highest current density, luminance and efficiency. The maximum luminance is 78850 cd m^{-2}, which is 88% enhanced from the planar device. And the current efficiency is 32.82 cd A^{-1}, which is 59% enhanced from the planar device. It should be noted that the current density for the corrugated OLED is also comparable higher than the planar device, which may be caused by the improved hole injection from the much smoother surface morphology of the imprinted anode. The operating OLEDs with planar and periodic anode (Imprinted Au) at the same driving voltage of 5 V are shown as inset in Fig. 4 (a), and much higher brightness can be observed from the corrugated OLEDs. The TM polarized EL spectra of the periodic device with different observing angles are presented in Fig. 4(c). The emission peaks show red shift and the emission intensity at longer wavelength is increased with the increasing observation angles, which is caused by the angular-dependent shift of the SPP resonance. On the other

hand, no angular dependence for the TE polarized EL spectra is observed (Fig. S6), due to the TM polarization of the SPP resonance.
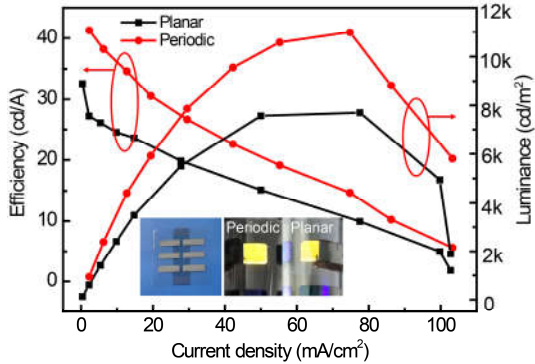

Fig. 5. The EL performance of planar and periodic OLEDs on flexible substrate. The inset shows the images of devices operating at 7V.

Ultrathin metallic film is especially suitable for the electrode of the flexible optoelectronic devices due to its excellent flexibility. The directly imprinting ultra-thin Au film is also suitable to fabricate the flexible OLEDs, and showing enhanced EL performance compared to the planar flexible OLEDs (Fig. 5). The directly imprinted microstructure can significantly increase the luminance from 7699 cd m^{-2} to 10990 cd m^{-2} and the current efficiency from 32.59 cd A^{-1} to 41.27 cd A^{-1}. Therefore, the imprinted metallic film is also applicable to the flexible OLEDs to outcouple the SPP loss and enhance the light extraction.

IV. CONCLUSIONS

In summary, the thermal nano-imprint lithography is employed to directly imprint periodic corrugation onto the surface of ultra-thin metallic film. And the surface morphology of ultrathin Au film is simultaneously improved during the imprinting of the corrugation on the Au film. The sheet resistance is decreased from 60 Ω sq^{-1} for the as-deposited planar Au film to 28 Ω sq^{-1} for the imprinted Au film with the periodic corrugation. The photons that trapped in SPP modes have been efficiently extracted by using the imprinted Au anode. The current efficiency is 59% enhanced from 20.69 cd A^{-1} to 32.82 cd A^{-1}. In addition, the imprinted metallic films are applicable to the flexible OLEDs, and improved current efficiency induced by the improved light extraction has been obtained.

ACKNOWLEDGEMENTS

REFERENCES

[1] Y. G. Bi, J. Feng, J. H. Ji, Y. Chen, Y. S. Liu, Y. F. Li, Y. F. Liu, X. L. Zhang, and H. B. Sun, "Ultrathin and ultrasmooth Au films as transparent electrodes in ITO-free organic light-emitting devices," *Nanoscale*, vol. 8, no. 19, pp. 10010-5, 2016.

[2] D. Yin, J. Feng, R. Ma, Y. F. Liu, Y. L. Zhang, X. L. Zhang, Y. G. Bi, Q. D. Chen, and H. B. Sun, "Efficient and mechanically robust stretchable organic light-emitting devices by a laser-programmable buckling process," *Nat Commun*, vol. 7, pp. 11573, 2016.

[3] R. Ding, X. P. Wang, J. Feng, X. B. Li, F. X. Dong, W. Q. Tian, J. R. Du, H. H. Fang, H. Y. Wang, T. Yamao, S. Hotta, and H. B. Sun, "Clarification of the Molecular Doping Mechanism in Organic Single-Crystalline Semiconductors and their Application in Color-Tunable Light-Emitting Devices," *Adv Mater*, vol. 30, no. 43, pp. e1801078, 2018.

[4] Y. Xu, X. Wei, C. Wang, J. Cao, Y. Chen, Z. Ma, Y. You, J. Wan, X. Fang, and X. Chen, "Silver Nanowires Modified with PEDOT: PSS and Graphene for Organic Light-Emitting Diodes Anode," *Sci Rep*, vol. 7, pp. 45392, 2017.

[5] D. Yin, J. Feng, N. R. Jiang, R. Ma, Y. F. Liu, and H. B. Sun, "Two-Dimensional Stretchable Organic Light-Emitting Devices with High Efficiency," *ACS Appl Mater Interfaces*, vol. 8, no. 45, pp. 31166-31171, 2016.

[6] C. C. Wu, C. I. Wu, J. C. Sturm, and A. Kahn, "Surface modification of indium tin oxide by plasma treatment: An effective method to improve the efficiency, brightness, and reliability of organic light emitting devices," *Applied Physics Letters*, vol. 70, no. 11, pp. 1348-1350, 1997.

[7] M. G. Helander, Z. B. Wang, J. Qiu, M. T. Greiner, D. P. Puzzo, Z. W. Liu, and Z. H. Lu, "Chlorinated indium tin oxide electrodes with high work function for organic device compatibility," *Science*, vol. 332, no. 6032, pp. 944-947, 2011.

[8] S. T. Lee, Z. Q. Gao, and L. S. Hung, "Metal diffusion from electrodes in organic light-emitting diodes," *Applied Physics Letters*, vol. 75, no. 10, pp. 1404-1406, 1999.

[9] W. H. Koo, S. M. Jeong, F. Araoka, K. Ishikawa, S. Nishimura, T. Toyooka, and H. Takezoe, "Light extraction from organic light-emitting diodes enhanced by spontaneously formed buckles," *Nature Photonics*, vol. 4, no. 4, pp. 222-226, 2010.

[10] G. Gustafsson, Y. Cao, G. M. Treacy, F. Klavetter, N. Colaneri, and A. J. Heeger, "Flexible light-emitting diodes made from soluble conducting polymers," *Cheminform*, vol. 24, no. 2, pp. 477-479, 1993.

[11] D. M. D. Leeuw, M. M. J. Simenon, A. R. Brown, and R. E. F. Einerhand, "Stability of n-type doped conducting polymers and consequences for polymeric microelectronic devices," *Synthetic Metals*, vol. 87, no. 1, pp. 53-59, 1997.

[12] R. Jonathan, I. Sahika, B. A. Collins, S. Michele, S. Eleni, S. Xenofon, T. Christopher, D. M. Delongchamp, and G. G. Malliaras, "Structural control of mixed ionic and electronic transport in conducting polymers," *Nature Communications*, vol. 7, pp. 11287, 2016.

[13] L. Zhou, M. Yu, X. Chen, S. Nie, W.-Y. Lai, W. Su, Z. Cui, and W. Huang, "Screen-Printed Poly(3,4-Ethylenedioxythiophene):Poly(Styrenesulfonate) Grids as ITO-Free Anodes for Flexible Organic Light-Emitting Diodes," *Advanced Functional Materials*, vol. 28, no. 11, pp. 1705955, 2018.

[14] P. Kang, K. H. Kim, H. G. Park, and S. Nam, "Mechanically reconfigurable architectured graphene for tunable plasmonic resonances," *Light Sci Appl*, vol. 7, pp. 17, 2018.

[15] Y. Xie, Y. Liu, Y. Zhao, Y. Tsang, S. Lau, H. Huang, and Y. Chai, "Stretchable all-solid-state supercapacitor with wavy shaped polyaniline/graphene electrode," *Journal of Materials Chemistry A*, vol. 2, no. 24, pp. 9142-9149, 2014.

[16] H. Park, S. Chang, X. Zhou, J. Kong, T. Palacios, and S. Gradečak, "Flexible Graphene Electrode-Based Organic Photovoltaics with Record-High Efficiency," *Nano Letters*, vol. 14, no. 9, pp. 5148-5154, 2015.

[17] X. Xu, H. Tan, K. Xi, S. Ding, D. Yu, S. Cheng, G. Yang, X. Peng, A. Fakeeh, and R. V. Kumar, "Bamboo-like amorphous carbon nanotubes clad in ultrathin nickel oxide nanosheets for lithium-ion battery electrodes with long cycle life," *Carbon*, vol. 84, no. 1, pp. 491-499, 2015.

[18] H. Li, K. Cao, J. Cui, S. Liu, X. Qiao, Y. Shen, and M. Wang, "14.7% efficient mesoscopic perovskite solar cells using single walled carbon nanotubes/carbon composite counter electrodes," *Nanoscale*, vol. 8, no. 12, pp. 6379-6385, 2016.

[19] S. Ye, A. R. Rathmell, Z. Chen, I. E. Stewart, and B. J. Wiley, "Metal nanowire networks: the next generation of transparent conductors," *Adv Mater*, vol. 26, no. 39, pp. 6670-87, 2014.

[20] B. Deng, P. C. Hsu, G. Chen, B. N. Chandrashekar, L. Liao, Z. Ayitimuda, J. Wu, Y. Guo, L. Lin, and Y. Zhou, "Roll-to-Roll Encapsulation of Metal Nanowires between Graphene and Plastic Substrate for High-Performance Flexible Transparent Electrodes," *Nano Letters*, vol. 15, no. 6, pp. 4206-4213, 2015.

[21] C. Zhang, D. Zhao, D. Gu, H. Kim, T. Ling, Y. K. Wu, and L. J. Guo, "An ultrathin, smooth, and low-loss Al-doped Ag film and its application as a

transparent electrode in organic photovoltaics," *Adv Mater*, vol. 26, no. 32, pp. 5696-701, 2014.

[22] J. Zou, C. Z. Li, C. Y. Chang, H. L. Yip, and A. K. Jen, "Interfacial engineering of ultrathin metal film transparent electrode for flexible organic photovoltaic cells," *Adv Mater*,vol. 26, no. 22, pp. 3618–3623, 2014.

[23] M. H. Grabow, and G. H. Gilmer, "Thin film growth modes, wetting and cluster nucleation," *Surface Science*, vol. 194, no. 3, pp. 333-346, 1988.

[24] L. Jiang, A. D. Wang, B. Li, T. H. Cui, and Y. F. Lu, "Electrons dynamics control by shaping femtosecond laser pulses in micro/nanofabrication: modeling, method, measurement and application," *Light Sci Appl*, vol. 7, pp. 17134, 2018.

[25] Daniel L. Becerra, a) Leah Y. Kuritzky,1 Joseph Nedy,2 Arwa Saud Abbas,1, R. M. F. Arash Pourhashemi, 1 Daniel A. Cohen,1 Steven P. DenBaars,1,2, and a. S. N. James S. Speck, 2, "Measurement and analysis of internal loss and injection efficiency for continuous-wave blue semipolar III-nitride laser diodes with chemically assisted ion beam etched facets," *Applied Physics Letters*, vol. 108, pp. 091106, 2016.

[26] Y. G. Bi, J. Feng, Y. F. Li, X. L. Zhang, Y. F. Liu, Y. Jin, and H. B. Sun, "Broadband light extraction from white organic light-emitting devices by employing corrugated metallic electrodes with dual periodicity," *Adv Mater*, vol. 25, no. 48, pp. 6969-74, Dec 23, 2013.

[27] H. H. Fudong Li, Jie Yin, Xuesong Jiang*, "Near-infrared light–responsive dynamic wrinkle patterns," Sci. Adv., vol. 4, pp. eaar5762, 2018.

[28] H. Wang, H.-Y. Wang, Q.-D. Chen, H.-L. Xu, H.-B. Sun, F. Huang, W. Raja, A. Toma, and R. Proietti Zaccaria, "Hybrid-State Dynamics of Dye Molecules and Surface Plasmon Polaritons under Ultrastrong Coupling Regime," *Laser & Photonics Reviews*, vol. 12, no. 3, pp. 1700176, 2018.

[29] Y.-F. L. Jing Feng, Yan-Gang Bi, and Hong-Bo Sun*, "Light manipulation in organic light-emitting devices by integrating micro/nano patterns," *Laser Photonics Rev.*, vol. 11, pp. 1600145, 2017.